Journal of Applied Physics

Influence of heat treatments in H_2 and Ar on the E_1 center in β-Ga_2O_3

Cite as: J. Appl. Phys. **131**, 115702 (2022); https://doi.org/10.1063/5.0083861
Submitted: 30 December 2021 • Accepted: 11 February 2022 • Published Online: 15 March 2022

Amanda Langørgen, Christian Zimmermann, Ymir Kalmann Frodason, et al.

Journal of Applied Physics ARTICLE scitation.org/journal/jap

Influence of heat treatments in H_2 and Ar on the E_1 center in β-Ga_2O_3

Cite as: J. Appl. Phys. **131**, 115702 (2022); doi: 10.1063/5.0083861
Submitted: 30 December 2021 · Accepted: 11 February 2022 ·
Published Online: 15 March 2022

View Online Export Citation CrossMark

Amanda Langørgen,[1,a)] Christian Zimmermann,[2] Ymir Kalmann Frodason,[1] Espen Førdestrøm Verhoeven,[1] Philip Michael Weiser,[1] Robert Michael Karsthof,[1] Joel Basile Varley,[3] and Lasse Vines[1]

AFFILIATIONS

[1]Department of Physics/Centre for Materials Science and Nanotechnology, University of Oslo, P.O. Box 1048, Blindern, Oslo N-0316, Norway
[2]Department of Physics, University of Washington, Seattle, Washington 98195, USA
[3]Lawrence Livermore National Laboratory, Livermore, California 94550, USA

Note: This paper is part of the Special Topic on Defects in Semiconductors.
[a)]**Author to whom correspondence should be addressed:** amandl@uio.no

ABSTRACT

The influence of heat treating *n*-type bulk β-Ga_2O_3 in hydrogen (H_2) and argon (Ar) gases on the presence of the defect level commonly labeled as E_1 was studied. Fourier transform-infrared spectroscopy confirms that hydrogen (H) is incorporated into β-Ga_2O_3 during H_2 annealing at 900 °C. Deep-level transient spectroscopy measurements reveal that the concentration of the E_1 level is promoted by the introduction of H, in contrast to what is observed in samples heat-treated in an Ar flow. We further find the E_1 level to be stable against heat treatments at 650 K, both with and without an applied reverse-bias voltage. Potential candidates for the defect origin of E_1 are investigated using hybrid-functional calculations, and three types of defect complexes involving H are found to exhibit charge-state transition levels compatible with E_1, including substitutional H at one of the threefold coordinated O sites, Ga-substitutional shallow donor impurities passivated by H, and certain configurations of singly hydrogenated Ga–O divacancies. Among these types, only the latter exhibit H binding energies that are consistent with the observed thermal stability of E_1.

I. INTRODUCTION

Monoclinic gallium sesquioxide (β-Ga_2O_3) is an ultra-wide bandgap semiconductor ($E_g \approx 4.9$ eV [1–3]) that has shown promise for applications in power electronics and UV photodetectors.[4–9] For β-Ga_2O_3 to live up to its potential, it is important to control the electrically active defects in the material since defects play a crucial role in determining the electrical conductivity of a semiconductor by acting as dopants or compensating centers.[10] Furthermore, defects can influence the operation of β-Ga_2O_3-based devices by, e.g., pinning the Fermi level[11–13] or acting as recombination centers.[14] Consequently, defect levels have been studied to a great extent in β-Ga_2O_3, using techniques such as electron paramagnetic resonance,[15–17] cathodoluminescence,[18,19] steady-state photo-capacitance,[20–30] and deep-level transient spectroscopy (DLTS).[11,12,22–24,26,31–36]

Recently, H-related defects in β-Ga_2O_3 have attracted considerable attention.[37–41] It has been shown in experimental and computational studies that Ga vacancies (V_{Ga}) complexed with H are likely to form in *n*-type material in the presence of H[42,43] and are expected to exhibit deep defect levels.[33,43] There are also a number of reports that propose H to be associated with shallow donor states,[38–40,44] potentially due to the formation of interstitial H (H_i) or H substituting for O (H_O).[45] Several other H-related defects have also been reported.[36,39,46–48]

The E_1 center is a DLTS defect signature with an activation energy of about 0.6 eV that has been observed previously in as-received bulk crystals grown by edge-defined film-fed growth (EFG) and the Czochralski (CZ) method,[31–33] as well as in epitaxial layers grown by molecular beam epitaxy (MBE)[49] and halide vapor phase epitaxy (HVPE).[23] Polyakov *et al.* observed an increase in the concentration of E_1 when subjecting EFG-grown bulk crystals with a surface orientation of (010) to a H-plasma,[50] whereas Irmscher *et al.* showed that the concentration of E_1 in CZ-grown bulk crystals was not increased by a high-temperature heat treatment in O_2 ambient.[31]

Different reports exist regarding the effect of irradiation on the E_1 level. Ingebrigtsen *et al.* and Farzana *et al.* did not observe any change in the E_1 concentration in EFG-grown bulk crystals, following 0.6 and 1.9 MeV proton,[33] and neutron irradiation,[28] suggesting that E_1 cannot be solely related to intrinsic defects. In contrast, Polyakov *et al.* reported a slight increase in the E_1 concentration following 20 MeV proton irradiation,[24] 18 MeV α-particle irradiation,[24] and pulsed fast reactor neutron irradiation[51] of HVPE films.

Here, we report on the effect of H_2 and Ar annealing on the E_1 level in EFG-grown bulk β-Ga_2O_3 crystals. The introduction of H into the crystals by annealing in H_2 is confirmed through Fourier transform-infrared spectroscopy (FT-IR) measurements, which reveal an O–H vibrational line previously assigned to a doubly hydrogenated Ga vacancy (V_{Ga}^{ib}2H).[42] From DLTS measurements, we find that H_2 heat treatments at 900 °C promote the concentration of E_1, whereas equivalent heat treatments performed in an inert Ar flow do not generate any notable changes in the E_1 concentration. We further find that the charge-carrier concentration is not influenced by H_2 heat treatments. Annealing at 650 K with and without an applied reverse-bias voltage revealed that the E_1 center is stable under these conditions. Finally, we discuss potential defect origins of the E_1 center based on comparison with hybrid-functional calculations on H-related defects in β-Ga_2O_3.

II. METHODS

Bulk EFG-grown β-Ga_2O_3 crystals[52,53] with a surface orientation of (−201) were purchased from Tamura Corporation,[54] including two different 0.7 mm thick wafers originating from different production batches. Both wafers were unintentionally doped *n*-type. The wafers were cut into samples measuring approximately $5 \times 5\,mm^2$ using a laser cutter.

Some of the samples were subjected to heat treatments in closed quartz ampoules filled with approximately 0.5 bar of H_2 at room temperature. The ampoules containing the samples were evacuated with a roughing pump prior to filling with H_2. Particularly, three cycles of evacuation and filling with H_2 were performed before eventually filling the ampoule with 0.5 bar of H_2 and subsequently sealing the ampoule. The heat treatments were performed in a tube furnace at a temperature of 900 °C for an annealing duration (t_{ann}) of 15–75 min. Once the furnace reached the set temperature, the ampoule containing the sample was put into the tube furnace, annealed for the desired duration, and then removed from the furnace to cool down. The samples were removed from the ampoules after they had reached room temperature; i.e., the samples were not exposed to air at elevated temperatures. In addition, three samples were subjected to heat treatments in an Ar flow at the same temperature of 900 °C for a t_{ann} between 15 and 60 min.

Using FT-IR, infrared absorbance spectra were measured at 5 K on as-received and both H_2- and Ar-annealed samples. The measurements were performed utilizing a Bruker IFS 125HR spectrometer equipped with a globar light source, a KBr beam splitter, and an InSb detector. The samples were cooled in a Janis PTSHI-950-5 closed-cycle, low vibration pulse tube cryostat filled with He exchange gas and equipped with ZnSe windows. All measurements used a spectral resolution of $0.5\,cm^{-1}$ with unpolarized light incident along the direction normal to the (−201) surface of the crystals. The single-channel spectrum of the empty sample holder was used as a reference. The recorded transmittance (Tr) data were converted to absorbance (A) using the equation $A = -\log_{10}(Tr)$.[55]

For the electrical characterization, Schottky barrier diodes (SBDs) were fabricated on samples in the as-received state or after H_2/Ar annealing. Circular Ni pads with diameters between 300 and 900 μm were deposited using e-beam evaporation and a shadow mask.[32,33,56] Typically, a contact thickness of 150 nm was used. Stacks of Ti (thickness = 10 nm) and Al (thickness = 150 nm) were used as Ohmic contacts covering the back side of the samples.

Current–voltage (IV) and capacitance–voltage (CV) measurements were performed in the dark on all SBDs to ensure that the devices were suitable for DLTS. IV measurements were performed using a Keithley 6487 picoammeter/voltage source, whereas CV measurements were conducted using a Boonton 7200 capacitance meter or an HP 4280A capacitance meter. From CV measurements, using a probing frequency of 1 MHz, the donor concentration (N_D) of the samples was determined[10] assuming a static dielectric constant of 10.2.[57] Moreover, the widths of the space-charge region (W), and hence the probing depths for DLTS measurements, were estimated from the CV measurements.[10]

DLTS measurements were performed on two setups, which both are refined setups of the one described in detail in Ref. 58, covering the temperature range from 150 to 700 K. The DLTS spectra were constructed using a GS2 filter (lock-in filter).[59] The spectra are displayed as $2N_D\Delta C/C_{rb}$, where ΔC denotes the amplitude of the capacitance transient measured in DLTS, whereas C_{rb} represents the quiescent capacitance of the SBD at the applied reverse-bias voltage.[10,60] Parameters describing the electron traps observed in DLTS measurements, such as the trap concentration (N_t), the activation energy (E_A), and the apparent capture cross section (σ_{na}), were obtained by comparing the recorded DLTS spectra with simulations using a python-based script.[20] Here, N_t was computed by taking the λ-correction into account.[10,20,31] The uncertainty in E_A is estimated to be around 0.04 eV, whereas the uncertainty in σ_{na} can be expected to be within $\pm$ one order of magnitude.[35]

To gauge the stability of the E_1 center, heat treatments of the 60 min H_2-annealed sample were performed. The annealing was conducted up to 650 K with and without an applied reverse-bias voltage of −5 V, denoted as reverse-bias annealing (RBA) and zero-bias annealing (ZBA), respectively. The annealing cycles were performed in the same manner as described in Ref. 36, except for a slower heating rate of 5 K/min and an HP 4280A capacitance meter as the voltage source.

First-principles calculations were performed using the projector augmented wave method[61,62] and the Heyd–Scuseria–Ernzerhof (HSE)[63] screened hybrid functional, as implemented in the VASP code.[64] The Ga 3*d* electrons were included in the valence, and the fraction of screened Hartree–Fock exchange was adjusted to 33%. This results in a direct bandgap value of 4.9 eV and lattice parameters ($a = 12.23$ Å, $b = 3.03$ Å, $c = 5.79$ Å, and $\beta = 103.8°$) in good agreement with experimental data.[1,65] Defect calculations were performed using 160-atom supercells, a plane-wave cutoff of 400 eV,

and a single special k-point at (0.25, 0.25, 0.25). Defect formation energies and thermodynamic charge-state transition levels were evaluated using the formalism described in Ref. 66, with finite-size corrections applied for charged defects.[67–69] Binding energies of H-related defect complexes were calculated as the difference between the formation energy of the complex and the sum of the formation energies of H_i and the remaining entity when one H is removed from the complex.[66] A positive binding energy indicates a stable complex.

To facilitate comparison between the hybrid-functional calculations and E_A extracted for E_1 from DLTS data, we have constructed one-dimensional configuration coordinate (CC) diagrams describing the dynamics of the electron capture and emission process.[70–72] CC model parameters were derived from the hybrid-functional calculations, including the ionization energy (E_i), the change in the configuration coordinate (ΔQ), and the ground and excited state Franck–Condon shifts (d_g^{FC} and d_e^{FC}). E_A extracted from DLTS includes an energetic barrier for electron capture (E_b) in addition to E_i. In the CC model, this barrier is obtained from the intersection point of the potential energy curves in the ground and excited state.[71]

III. RESULTS AND DISCUSSION

A. Incorporation of hydrogen and electrical properties

Figure 1 shows baseline-corrected IR absorbance spectra recorded on as-received and H_2-annealed samples. The baseline in the absorbance spectra originates from surface reflection losses, scattering at the rough back surface, and free charge-carrier absorption.[42] The samples annealed in H_2 exhibit an absorbance feature at around 3437 cm^{-1}, which is related to a localized vibrational mode (LVM) associated with $V_{Ga}^{ib}2H$.[42] Indeed, $V_{Ga}^{ib}2H$ has previously been found to form under n-type conditions during H_2 annealing,[42] in line with first-principles calculations.[33,43] The as-received and Ar-annealed samples did not show such an absorbance feature (FT-IR data for samples annealed in Ar are not shown), indicating that $V_{Ga}^{ib}2H$ is only present in negligible amounts in the bulk of these samples. The data were modeled with Lorentzian profiles to compute the integrated absorbance of the feature related to the LVM of $V_{Ga}^{ib}2H$. The integrated absorbance is proportional to the concentration of $V_{Ga}^{ib}2H$ in the bulk crystals, and hence, an approximately linear relation between the $V_{Ga}^{ib}2H$ concentration and t_{ann} can be seen in the inset of Fig. 1. Thus, the results displayed in Fig. 1 show that H penetrates into the bulk of β-Ga_2O_3 during H_2 annealing. However, the concentration of H is too low to be measured by, e.g., chemical techniques, such as secondary ion mass spectrometry. Note that the small shoulder that can be discerned at 3439.5 cm^{-1} in Fig. 1 is caused by noise in the baseline.

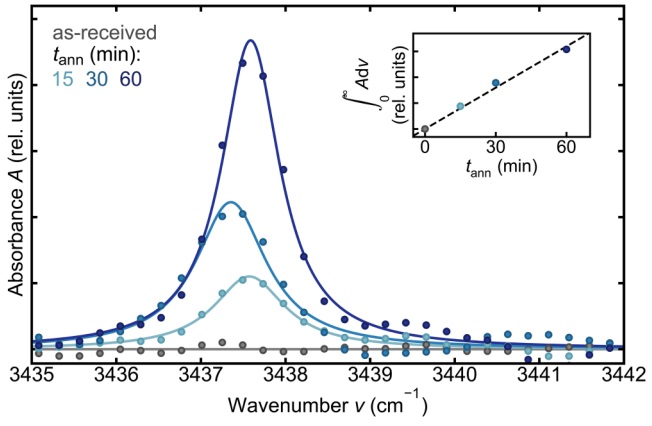

FIG. 1. Baseline-corrected IR absorbance spectra recorded on as-received and H_2-annealed EFG β-Ga_2O_3 bulk crystals. The data (full circles) were modeled with Lorentzian profiles (solid lines) to extract the integrated absorbance of the feature at around 3437 cm^{-1}, which is related to a LVM associated with $V_{Ga}^{ib}2H$.[42] The inset shows the dependence of the integrated baseline-corrected absorbance on t_{ann}.

IV and CV measurements on SBDs comprising as-received, H_2-annealed, and Ar-annealed samples showed that the SBDs were suitable for performing DLTS measurements. In IV measurements, SBDs fabricated on H_2-annealed samples typically displayed a larger leakage current (current under an applied reverse-bias voltage) compared to as-received and Ar-annealed samples. This limited the t_{ann} that could be used for the H_2 heat treatments. The increase in leakage current might be related to roughening of the sample surface during the H_2 annealing.[39,50]

From CV measurements, N_D values between 2×10^{17} and 5×10^{17} cm^{-3} were determined for all samples independent of the heat treatment. The values determined for N_D indicate that the Fermi level is close to E_C in all investigated samples. From CV measurements, the typical probing depth for DLTS measurements is determined to be in the range of 150–250 nm. Notably, no correlation between t_{ann} and N_D was observed for neither the H_2 nor the Ar annealing. However, the as-received samples displayed a considerable spread in N_D, and hence, a possible correlation between t_{ann} and N_D might be masked. Previously, Polyakov *et al.* have shown that surface treatments with H-plasma lead to an increase in carrier concentration for EFG-grown bulk crystals with a (−201) surface orientation, which the authors proposed to be related to the formation of shallow H-related donors.[50] Interestingly, H-plasma treatments caused a decrease in carrier concentration for EFG-grown bulk crystals with a (010) surface orientation.[38,50] This might be a result of distinct surface terminations on the (−201) and (010) surfaces resulting from H treatment that influence the surface band bending.[41] It has also been shown that H can contribute to the unintentional doping found in as-grown bulk crystals.[40]

B. E_1 concentration and stability

DLTS spectra recorded on as-received, 30 min H_2-annealed, and 30 min Ar-annealed crystals are presented in Fig. 2. The E_1 peak ($E_A = 0.60 \pm 0.04$ eV, $\sigma_{na} \sim 6\times10^{-13}$ cm^2) is present in all three spectra (see the inset in Fig. 2 to discern the peak for the as-received and Ar-annealed sample). At temperatures of around 280 K, the onset of a signature commonly labeled as E_2 can be seen, which has previously been shown to be related to substitutional Fe at tetrahedral Ga1 and octahedral Ga2 sites (Fe_{Ga1} and Fe_{Ga2}).[20,32,35] Notably, we did not observe the center commonly

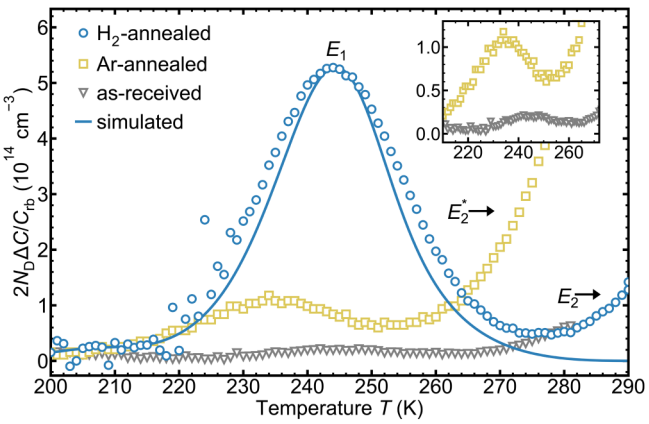

FIG. 2. DLTS spectra recorded on as-received, H_2-, and Ar-annealed EFG-grown β-Ga_2O_3 bulk crystals. The rate window is (640 ms)$^{-1}$. The data for the H_2-annealed sample (circles) are modeled with a simulation (solid line). The H_2 and Ar anneals were both performed at 900 °C for 30 min. The observed defect signatures are labeled. The inset shows the E_1 peak for the as-received and Ar-annealed samples. The axes units of the inset are the same as for the main plot.

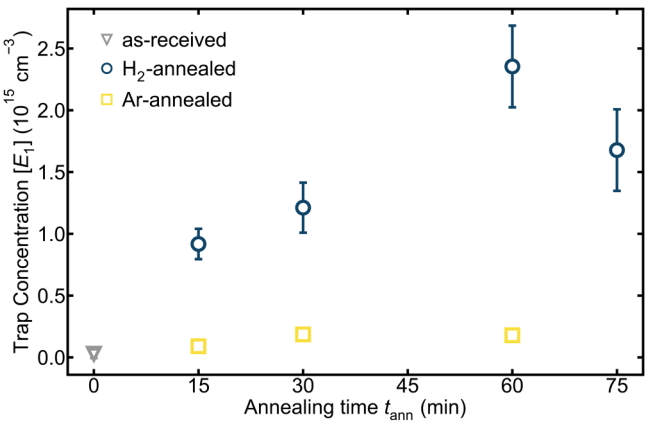

FIG. 3. Mean and standard deviation values of the E_1 concentration ($[E_1]$) extracted from DLTS measurements on as-received, H_2-, and Ar-annealed EFG-grown bulk crystals in dependence of t_{ann}. The λ-correction was taken into account for computing $[E_1]$.

labeled as E_2^* after H_2 anneals.[11,23,32,33,36] For Ar anneals, however, a defect level around E_2^* appears as a small shoulder on the low-temperature side of E_2 (its onset can be seen around 260 K in Fig. 2).

For the spectra presented in Fig. 2, the concentration of the E_1 level is comparable for the as-received and Ar-annealed samples but considerably higher for the sample annealed in H_2. Note that the peak position of the DLTS signature in the Ar-annealed sample is shifted to lower temperatures compared to that of the E_1 level, which may indicate that Ar annealing results in the formation of other defect levels with a similar energy level position. Moreover, the DLTS signature of E_1 (Fig. 2) is somewhat broader than that expected from a single level, as indicated by the simulated line. Thus, we cannot exclude that E_1 consists of several overlapping levels. However, we were not able to resolve a finer structure in the E_1 peak with the use of the high-resolution weighting function GS4.[59]

Figure 3 shows the E_1 concentration in dependence of t_{ann} obtained from multiple DLTS measurements recorded on as-received, Ar-annealed, and H_2-annealed samples. For the as-received and H_2-annealed samples, the mean and standard deviation values are calculated from several diodes (between 3 and 14, the latter to check for lateral inhomogeneity) for the different t_{ann}. Note that the 15 and 60 min H_2 annealing was performed solely on a single wafer, whereas the 75 min annealing was performed on a different wafer.

From Fig. 3, one can observe that the mean E_1 concentration in as-received bulk crystals is low. Indeed, for some of the diodes on the as-received bulk crystals, the E_1 concentration was below the detection limit of around 5×10^{12} cm^{-3} and thus not observed in the DLTS measurements. The diodes on the as-received samples that displayed the presence of E_1 had an N_t of around 5×10^{13} cm^{-3} taking the λ-correction into account. The samples annealed in argon similarly displayed a low E_1 concentration of around $1{\times}10^{14}$ cm^{-3}. Moreover, the Ar-annealed samples do not show a systematic increase in the E_1 concentration with increasing t_{ann}. For the Ar-annealed samples, it should be noted that the E_1 concentration was extracted treating the shifted peaks as pertaining to E_1, and hence, the calculated concentrations can be considered an upper bound. The samples annealed in H_2, in contrast, display a considerably larger concentration of E_1 in the range of $1{\times}10^{15}$ cm^{-3}. For annealing times up to and including 60 min, the mean E_1 concentration also increases with increased time.

For the sample annealed in H_2 for 75 min, a slightly lower concentration of E_1 is measured compared to that of the 60 min ones but still substantially above that of the as-received. This may indicate that for long annealing times, multiple defect reactions may influence the overall E_1 concentration. In addition, as the 60 min-annealed and 75 min-annealed diodes stem from two separate wafers, initial differences in the relative and absolute defect concentrations can affect the resulting E_1 concentration. Nevertheless, the results displayed in Figs. 2 and 3 lead us to propose that E_1 is associated with a H-related defect.

Probing the thermal and field dependent stability of defect levels can provide valuable information for the identification of defects. Several defect levels in β-Ga_2O_3 have previously been shown to be metastable[36,49] with the use of RBA and ZBA. For example, we have previously found that E_2^* formed by H implantation can be reversibly introduced and removed by performing RBA and ZBA, respectively, at temperatures of around 650 K.[36] Figure 4 shows the results for the E_1 level following RBA and ZBA cycles. More specifically, DLTS spectra recorded after 60 min H_2 annealing and after subsequent RBA and ZBA at 650 K are presented. A notable finding is that the peak intensity shows an insignificant change after the annealing cycles. The unchanged intensity suggests that E_1 is related to a stable defect. We observe only a slight

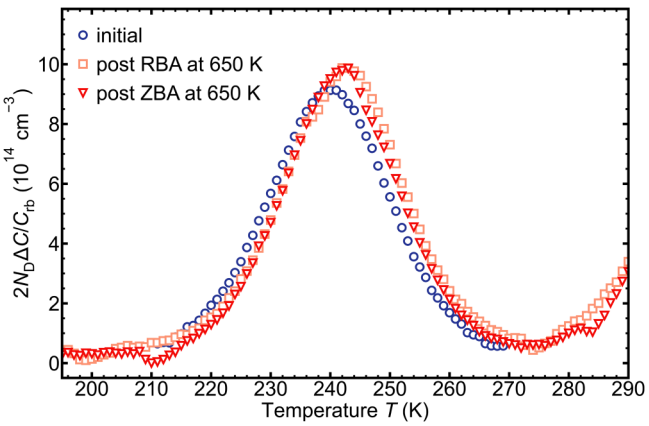

FIG. 4. DLTS spectra recorded on a sample annealed in H_2 for a duration of 60 min. The initial DLTS spectra and the DLTS spectra following RBA and ZBA at 650 K are shown. The rate window is $(640\text{ms})^{-1}$.

increase (decrease) in the peak intensity (temperature position) of the E_2 signature, following RBA and no further change following ZBA. Furthermore, no distinct shoulder, which would correspond to E_2^*, emerges on the low-temperature side of E_2 after RBA at 650 K.

C. Results of first-principles calculations

Hybrid-functional calculations were performed to explore potential defects that might give rise to the E_1 center, assuming a H-related origin. Previous calculations indicate that H_i behaves exclusively as a shallow donor in β-Ga_2O_3, as the predicted $\varepsilon(+/-)$ level is close to E_C.[45] Isolated H could also occur in the form of interstitial molecular hydrogen $(H_2)_i$, which we find to be electrically inactive and stable only in n-type material with a maximum binding energy of 0.85 eV. However, H_i and $(H_2)_i$ are expected to be highly mobile.[45] Indeed, using the climbing-image nudged elastic band method[73] and the strongly constrained and appropriately normed semilocal functional,[74] we calculate migration barriers along the b axis of 0.24 and 0.61 eV for H_i and $(H_2)_i$, respectively. For this reason, H most likely occurs in a trapped form, such as a defect complex involving an intrinsic defect or possibly another impurity; Si, Al, Fe, and Ir are commonly found in EFG-grown β-Ga_2O_3 crystals.[32,75]

Figures 5(a) and 5(b) show the formation and binding energy diagrams, respectively, of various H-related defect complexes exhibiting charge-state transition levels in the vicinity of E_1, as discussed below. The formation energies of other defects mentioned below are reported elsewhere.[33,45,76,77] The notation used for the defects is in accordance with Ref. 77.

We start by considering intrinsic defects that can trap H. Previous calculations have shown that H can be trapped by V_O, resulting in a H_O complex that behaves as a shallow donor.[45] Interestingly, we find that the H_{O2} configuration can be stabilized also in the single-negative charge state for Fermi-level positions close to E_C (see Fig. 5). As shown in Fig. 6, the single-negative charge state involves a large structural rearrangement, where H moves off the vacant threefold coordinated O2 site to form a bond with the adjacent Ga2 atom, and two electrons are captured in a localized state. Note that charge-neutral H_{O_2} is unstable for any position of the Fermi level, resulting in negative-U behavior;[78] i.e., the thermodynamic charge-state transition occurs directly from single positive to single negative in Fig. 5(a). For a negative-U center, the peak observed in a conventional DLTS spectrum will correspond to the emission of two electrons, but E_A will be

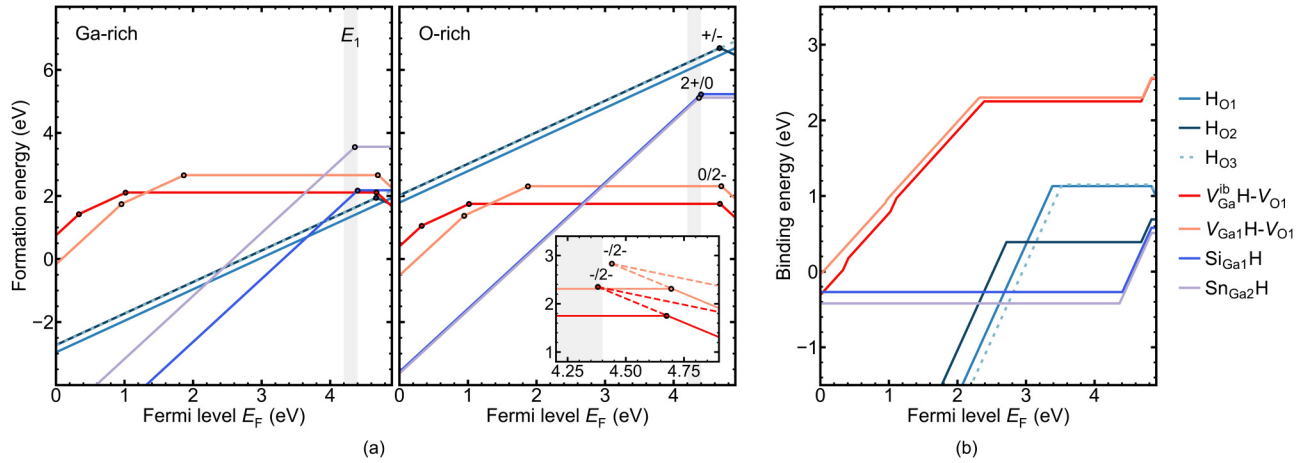

FIG. 5. (a) Calculated formation energies under (left) Ga-rich and (right) O-rich conditions of various H-related defect complexes in β-Ga_2O_3. These defects display thermodynamic charge-state transition levels that are close in Fermi-level position to the measured E_A for E_1 (gray vertical bar 0.6 eV $\pm$ 0.1 eV below E_C). Note that all corresponding transitions show negative-U behavior. The inset shows the $-/2-$ transitions for the singly hydrogenated Ga–O divacancies. The axes units of the inset are the same as for the main plot. (b) Calculated binding energies for the H-related complexes.

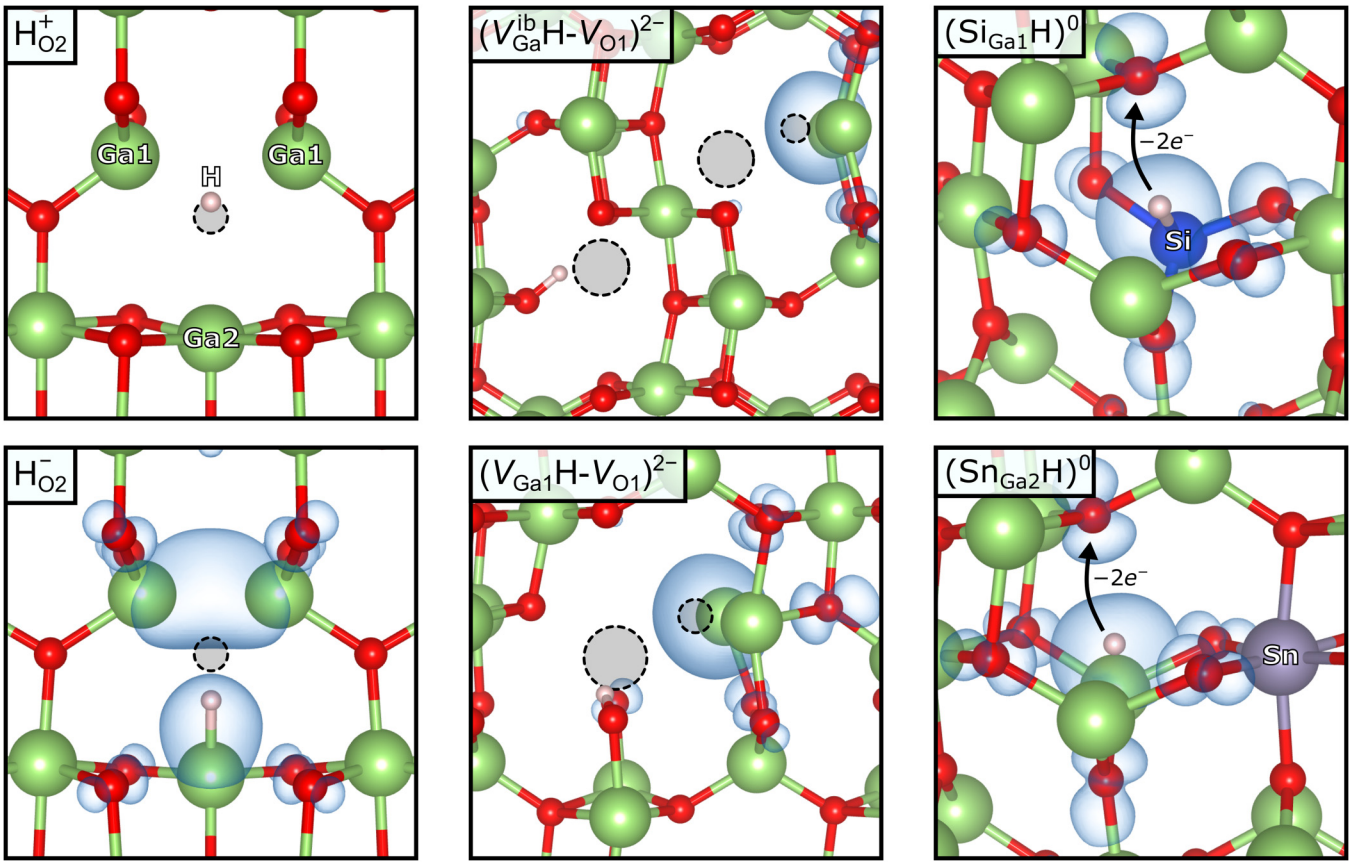

FIG. 6. Relaxed structures of the H-related defect complexes discussed as potential E_1 origins. The transition from the + to the − charge state of H_{O2} corresponds to H moving off the vacant O2 site to form a bond with the adjacent Ga2 atom, allowing two electrons to be trapped in a localized defect state (blue isosurface). For the $(Si_{Ga1}H)^0$ and $(Sn_{Ga2}H)^0$ complexes, the arrows indicate the O site where an O–H bond is formed for their 2+ charge states in Fig. 5.

determined by the first electron emission, corresponding to the $\varepsilon(0/-)$ level for H_{O_2}.[79]

As shown in Table I, the corresponding E_i value for H_{O2} is 0.68 eV with a small E_b of 0.10 eV, which is close to the measured E_A of ∼0.6 eV for E_1. However, H_{O2} is expected to show a low thermal stability, with a maximum binding energy of 0.69 eV when the Fermi-level position is near E_C, as shown in Fig. 5(b).

TABLE I. Calculated CC model parameters for the process of nonradiative emission of an electron from different defect complexes involving H to E_C, including E_i, E_b, d_{FC}^{g}, d_{FC}^{e}, and ΔQ.

Defect and transition	E_i (eV)	E_b (eV)	$d_{FC}^{g/e}$ (eV)	ΔQ (amu$^{1/2}$Å)
H_{O2} (0/−)	0.68	0.10	1.45 / 1.53	2.78
$V_{Ga}^{ib}H\text{–}V_{O1}$ (−/2−)	0.52	0.19	1.48 / 2.01	5.59
$V_{Ga1}H\text{–}V_{O1}$ (−/2−)	0.49	0.20	1.46 / 2.03	6.41
$Si_{Ga1}H$ (+/0)	≤0.99	…	…	…
$Sn_{Ga2}H$ (+/0)	≤1.07	…	…	…

Combining this with the low H_i migration barrier, one would thus expect H_{O2} to dissociate relatively easily.[33] This is hard to reconcile with the apparent stability of E_1 upon ZBA and RBA up to 650 K.

As a donor, H_i is particularly likely to form stable complexes with acceptors, such as V_{Ga}.[33,80] Indeed, the main O–H vibrational line observed by FT-IR in the hydrogen-annealed material is caused by $V_{Ga}^{ib}2H$.[42] However, the calculated thermodynamic charge-state transition levels of V_{Ga} are located in excess of 1.8 eV below E_C, and complexing with H tends to shift these levels to even lower Fermi-level positions.[33]

Another possibility is Ga–O divacancies ($V_{Ga}V_O$), which exhibit negative-U $\varepsilon(-/3-)$ levels in the upper part of the bandgap that are associated with the formation of Ga–Ga dimers at V_O.[33,77] $V_{Ga}V_O$ can occur in a large number of crystallographically inequivalent configurations. However, the negative-U charge-state transition levels tend to (i) cluster within narrow ranges of Fermi-level positions, depending on the combination of tetrahedral Ga1 and octahedral Ga2 in the dimer, and (ii) shift to lower Fermi-level positions when $V_{Ga}V_O$

is hydrogenated.[77] We have previously discussed certain configurations of the isolated and doubly hydrogenated $V_{Ga}V_O$ as potential defect origins of the E_2^* center.[77] As shown in Fig. 5, we find that the singly hydrogenated divacancies V_{Ga}^{ib}H–V_{O1} and V_{Ga1}H–V_{O1} exhibit $\varepsilon(0/2-)$ levels that are close to E_C and E_1 (four additional configurations with similar level positions can be found in Ref. 77, but these are not included here as they are higher in energy). As shown in Fig. 6, the 2- charge state correspond to the formation of a Ga2–Ga2 dimer at V_{O1}. In this case, $\varepsilon(-/2-)$ is the relevant level for comparison with DLTS, and the corresponding E_i (E_b) values are 0.52 (0.19) and 0.49 (0.20) eV for V_{Ga}^{ib}H–V_{O1} and V_{Ga1}H–V_{O1}, respectively. These energies are also compatible with E_1.

In contrast to the H_{O2} complex, V_{Ga}^{ib}H–V_{O1} and V_{Ga1}H–V_{O1} are expected to show high thermal stability, with binding energies in excess of 2.2 eV under n-type conditions, as shown in Fig. 5(b). These binding energies are comparable to the 2.62 eV predicted for V_{Ga}^{ib}2H.[80] Furthermore, the possibility of E_1 being composed of several overlapping defects is in agreement with this defect model, as there are several configurations of the singly hydrogenated divacancy exhibiting similar activation energies.[77]

It should be noted that the V_{Ga2}H–V_{O2} and V_{Ga}^{ia}H–V_{O2}^{b} configurations, which have the $\varepsilon(0/2-)$ level at ~1.7 eV below E_C, are ~0.4 eV lower in formation energy than V_{Ga}^{ib}H–V_{O1} when $E_F = E_C$.[77] V_{Ga}^{ib}H–V_{O1} becomes preferred when the Fermi-level position is below $E_C - 0.46$ eV.[77] Moreover, a second H can be trapped by V_{Ga}^{ib}H–V_{O1}, resulting in the V_{Ga}^{ib}H–H_{O1} configuration when $E_F = E_C$. The V_{Ga}^{ib}H–H_{O1} complex has a H binding energy of 2.34 eV and does not exhibit any levels in the vicinity of E_1. For these reasons, the concentration of V_{Ga}^{ib}H–V_{O_i} (and other E_1 compatible configurations), relative to divacancies in other configurations and with different numbers of H, can be expected to depend on several factors, such as the concentration ratio of H to $V_{Ga}V_O$ and other traps, the Fermi-level position, the temperature, and the energy barriers associated with transformations between different isolated and hydrogenated $V_{Ga}V_O$ configurations.[77,81]

Finally, we consider complexes between H and other common impurities in β-Ga_2O_3. An obvious candidate is the Fe_{Ga} acceptor (E_2), which displays $\varepsilon(0/-)$ levels at 0.6-0.7 eV below E_C.[20,32,35] However, Varley[76] calculated a binding energy of 0.7 eV for the Fe_{Ga2}H complex and a $\varepsilon(+/0)$ level located 1.3 eV below E_C.[76] Similarly, polaronic acceptor impurities, such as Mg, exhibit even deeper levels that are also shifted to lower Fermi-level positions when hydrogenated.[82,83] Polyakov *et al.*[38] have suggested that H can passivate shallow donor impurities by forming charge-neutral complexes. We have investigated this possibility for silicon and tin donors in their most favorable configuration, Si_{Ga1} and Sn_{Ga2} (Sn is a commonly used n-type dopant and is included for comparison). Although cationic H_i^+ is the energetically preferred form of isolated H, we indeed find that anionic H_i^- can be stabilized in the vicinity of these Ga substitutional shallow donor impurities, resulting in charge-neutral Si_{Ga1}H and Sn_{Ga2}H pairs under n-type conditions, as shown in Fig. 5(a). However, formation of these complexes might be suppressed by screened Coulomb repulsion, as both constituents are positively charged for any position of the Fermi level in the bandgap. Moreover, these complexes are only stable in n-type material, with modest binding energies of up to 0.58 and 0.51 eV for Si_{Ga1}H and Sn_{Ga2}H, respectively, as shown in Fig. 5(b). Additionally, their stability rapidly decreases with the Fermi level, indicating likely complex dissociation under RBA conditions. For lower Fermi-level positions, H_i^+ is preferred over H_i^-, also in the vicinity of the donor. Indeed, the 2+ charge states shown in Fig. 5 correspond to a H_i^+ immediately adjacent to Si_{Ga}^+ or Sn_{Ga}^+ (H forms a bond with the O indicated by arrows in Fig. 6). The single-positive charge state of the complex is similar but has an electron occupying a delocalized perturbed host state[66] just below E_C. This prevents an accurate evaluation of $\varepsilon(+/0)$, as the 160-atom supercell is not sufficiently large for such spatially extended defect states.[84] The upper estimates of ~1 eV in Table I assume a donor ionization energy of zero, which corresponds to the $\varepsilon(2+/+)$ level being located at E_C. Nonetheless, the low thermal and bias-induced stability of these donor complexes are incompatible with those observed for E_1.

IV. SUMMARY AND CONCLUSION

In summary, we have investigated the influence of H_2 and Ar annealing of n-type EFG-grown β-Ga_2O_3 on the presence of the E_1 center. Using FT-IR, we confirmed that H is incorporated into the bulk crystals during H_2 heat treatments. Notably, the H_2 heat treatments did not lead to any considerable changes in charge-carrier concentration. Using DLTS, it was shown that the H_2 annealing promotes the defect level E_1, suggesting a H-related defect origin for the E_1 center. Based on comparison with hybrid-functional calculations for defect complexes involving H, specific defect origins of E_1 are discussed. We find three different types of H-related defects exhibiting charge-state transition levels and capture barriers that are compatible with the measured activation energy for E_1, including (i) the $\varepsilon(+/-)$ level of H_{O2}, (ii) the $\varepsilon(-/2-)$ level of singly hydrogenated Ga–O divacancies exhibiting Ga2–Ga2 dimers (V_{Ga}^{ib}H–V_{O1} and V_{Ga1}H–V_{O1} being the lowest energy configurations),[77] and (iii) the $\varepsilon(+/0)$ level of Ga substitutional shallow donor impurities passivated by anionic H_i^-, e.g., Si_{Ga1}H and Sn_{Ga2}H. Among these defect candidates, only (ii) is consistent with the apparent stability of E_1 upon RBA and ZBA up to 650 K.

ACKNOWLEDGMENTS

Financial support is acknowledged from the Research Council of Norway through the GO2DEVICE project (Project No. 301740), the FUNDAMeNT project (Project No. 251131), the GO-POW project (Project No. 314017), the Norwegian Micro- and Nano-Fabrication Facility (NorFab, Project No. 295864), and the Faculty of Mathematics and Natural Sciences at the University of Oslo via the strategic research initiative FOXHOUND. Funding for this work was also provided by the Norwegian Research Council through the Research Center for Sustainable Solar Cell Technology (FME SUSOLTECH, Project No. 257639). This work was partially performed under the auspices of the U.S. DOE by the Lawrence Livermore National Laboratory (LLNL) under Contract No. DE-AC52-07NA27344 and partially supported by the LLNL Laboratory Directed Research and Development funding under Project No. 22-SI-003 and by the Critical Materials Institute, an

Energy Innovation Hub funded by the U.S. DOE, Office of Energy Efficiency and Renewable Energy, Advanced Manufacturing Office.

AUTHOR DECLARATIONS

Conflict of Interest

The authors have no conflicts to disclose.

DATA AVAILABILITY

The data that support the findings of this study are available from the corresponding author upon reasonable request.

REFERENCES

[1]C. Janowitz, V. Scherer, M. Mohamed, A. Krapf, H. Dwelk, R. Manzke, Z. Galazka, R. Uecker, K. Irmscher, and R. Fornari *et al.*, New J. Phys. **13**, 085014 (2011).
[2]T. Onuma, S. Saito, K. Sasaki, K. Goto, T. Masui, T. Yamaguchi, T. Honda, A. Kuramata, and M. Higashiwaki, Appl. Phys. Lett. **108**, 101904 (2016).
[3]T. Onuma, S. Saito, K. Sasaki, T. Masui, T. Yamaguchi, T. Honda, and M. Higashiwaki, Jpn. J. Appl. Phys. **54**, 112601 (2015).
[4]M. Higashiwaki, K. Sasaki, H. Murakami, Y. Kumagai, A. Koukitu, A. Kuramata, T. Masui, and S. Yamakoshi, Semicond. Sci. Technol. **31**, 034001 (2016).
[5]S. Nakagomi, T. Momo, S. Takahashi, and Y. Kokubun, Appl. Phys. Lett. **103**, 072105 (2013).
[6]S. Nakagomi, T. Sato, Y. Takahashi, and Y. Kokubun, Sens. Actuator A Phys. **232**, 208 (2015).
[7]M. A. Mastro, A. Kuramata, J. Calkins, J. Kim, F. Ren, and S. Pearton, ECS J. Solid State Sci. Technol. **6**, P356 (2017).
[8]Z. Galazka, Semicond. Sci. Technol. **33**, 113001 (2018).
[9]S. J. Pearton, J. Yang, P. H. Cary, F. Ren, J. Kim, M. J. Tadjer, and M. A. Mastro, Appl. Phys. Rev. **5**, 011301 (2018).
[10]P. Blood and J. Orton, *The Electrical Characterization of Semiconductors: Majority Carriers and Electron States* (Academic Press, 1992).
[11]J. F. Mcglone, Z. Xia, Y. Zhang, C. Joishi, S. Lodha, S. Rajan, S. A. Ringel, and A. R. Arehart, IEEE Electron Device Lett. **39**, 1042 (2018).
[12]J. F. McGlone, Z. Xia, C. Joishi, S. Lodha, S. Rajan, S. Ringel, and A. R. Arehart, Appl. Phys. Lett. **115**, 153501 (2019).
[13]S.-S. Huang, R. Lopez, S. Paul, A. T. Neal, S. Mou, M.-P. Houng, and J. V. Li, Jpn. J. Appl. Phys. **57**, 091101 (2018).
[14]L. Huang, Q. Feng, G. Han, F. Li, X. Li, L. Fang, X. Xing, J. Zhang, and Y. Hao, IEEE Photon. J. **9**, 6803708 (2017).
[15]S. Bhandari and M. E. Zvanut, J. Appl. Phys. **127**, 065704 (2020).
[16]S. Bhandari, M. E. Zvanut, and J. B. Varley, J. Appl. Phys. **126**, 165703 (2019).
[17]C. A. Lenyk, T. D. Gustafson, L. E. Halliburton, and N. C. Giles, J. Appl. Phys. **126**, 245701 (2019).
[18]H. Gao, S. Muralidharan, N. Pronin, M. R. Karim, S. M. White, T. Asel, G. Foster, S. Krishnamoorthy, S. Rajan, L. R. Cao, M. Higashiwaki, H. von Wenckstern, M. Grundmann, H. Zhao, D. C. Look, and L. J. Brillson, Appl. Phys. Lett. **112**, 242102 (2018).
[19]H. Gao, S. Muralidharan, M. R. Karim, S. M. White, L. R. Cao, K. Leedy, H. Zhao, D. C. Look, and L. J. Brillson, J. Phys. D: Appl. Phys. **53**, 465102 (2020).
[20]C. Zimmermann, Y. K. Frodason, V. Rønning, J. B. Varley, and L. Vines, New J. Phys. **22**, 063033 (2020).
[21]C. Zimmermann, V. Rønning, Y. K. Frodason, V. Bobal, L. Vines, and J. B. Varley, Phys. Rev. Mater. **4**, 074605 (2020).
[22]E. Farzana, E. Ahmadi, J. S. Speck, A. R. Arehart, and S. A. Ringel, J. Appl. Phys. **123**, 161410 (2018).
[23]A. Y. Polyakov, N. B. Smirnov, I. V. Shchemerov, E. B. Yakimov, J. Yang, F. Ren, G. Yang, J. Kim, A. Kuramata, and S. J. Pearton, Appl. Phys. Lett. **112**, 032107 (2018).
[24]A. Y. Polyakov, N. B. Smirnov, I. V. Shchemerov, E. B. Yakimov, S. J. Pearton, C. Fares, J. Yang, F. Ren, J. Kim, P. B. Lagov, V. S. Stolbunov, and A. Kochkova, Appl. Phys. Lett. **113**, 092102 (2018).
[25]Z. Zhang, E. Farzana, A. R. Arehart, and S. A. Ringel, Appl. Phys. Lett. **108**, 052105 (2016).
[26]A. Y. Polyakov, N. B. Smirnov, I. V. Shchemerov, D. Gogova, S. A. Tarelkin, and S. J. Pearton, J. Appl. Phys. **123**, 115702 (2018).
[27]A. Y. Polyakov, N. B. Smirnov, I. V. Shchemerov, S. J. Pearton, F. Ren, A. V. Chernykh, and A. I. Kochkova, Appl. Phys. Lett. **113**, 142102 (2018).
[28]E. Farzana, M. F. Chaiken, T. E. Blue, A. R. Arehart, and S. A. Ringel, APL Mater. **7**, 022502 (2019).
[29]Y. Nakano, ECS J. Solid State Sci. Technol. **6**, P615 (2017).
[30]H. Ghadi, J. F. McGlone, C. M. Jackson, E. Farzana, Z. Feng, A. F. M. A. U. Bhuiyan, H. Zhao, A. R. Arehart, and S. A. Ringel, APL Mater. **8**, 021111 (2020).
[31]K. Irmscher, Z. Galazka, M. Pietsch, R. Uecker, and R. Fornari, J. Appl. Phys. **110**, 063720 (2011).
[32]M. E. Ingebrigtsen, J. B. Varley, A. Y. Kuznetsov, B. G. Svensson, G. Alfieri, A. Mihaila, U. Badstübner, and L. Vines, Appl. Phys. Lett. **112**, 042104 (2018).
[33]M. E. Ingebrigtsen, A. Y. Kuznetsov, B. G. Svensson, G. Alfieri, A. Mihaila, U. Badstübner, A. Perron, L. Vines, and J. B. Varley, APL Mater. **7**, 022510 (2019).
[34]A. Y. Polyakov, N. B. Smirnov, I. V. Shchemerov, S. J. Pearton, F. Ren, A. V. Chernykh, P. B. Lagov, and T. V. Kulevoy, APL Mater. **6**, 096102 (2018).
[35]C. Zimmermann, Y. K. Frodason, A. W. Barnard, J. B. Varley, K. Irmscher, Z. Galazka, A. Karjalainen, W. E. Meyer, F. D. Auret, and L. Vines, Appl. Phys. Lett. **116**, 072101 (2020).
[36]C. Zimmermann, E. F. Verhoeven, Y. K. Frodason, P. M. Weiser, J. B. Varley, and L. Vines, J. Phys. D: Appl. Phys. **53**, 464001 (2020).
[37]M. M. Islam, M. O. Liedke, D. Winarski, M. Butterling, A. Wagner, P. Hosemann, Y. Wang, B. Uberuaga, and F. A. Selim, Sci. Rep. **10**, 6134 (2020).
[38]A. Y. Polyakov, I.-H. Lee, N. B. Smirnov, E. B. Yakimov, I. V. Shchemerov, A. V. Chernykh, A. I. Kochkova, A. A. Vasilev, F. Ren, P. H. Carey, and S. J. Pearton, Appl. Phys. Lett. **115**, 032101 (2019).
[39]Y. Qin, M. Stavola, W. B. Fowler, P. Weiser, and S. J. Pearton, ECS J. Solid. State. Sci. **8**, Q3103 (2019).
[40]Z. Galazka, K. Irmscher, R. Schewski, I. M. Hanke, M. Pietsch, S. Ganschow, D. Klimm, A. Dittmar, A. Fiedler, T. Schroeder, and M. Bickermann, J. Cryst. Growth **529**, 125297 (2020).
[41]J. E. N. Swallow, J. B. Varley, L. A. H. Jones, J. T. Gibbon, L. F. J. Piper, V. R. Dhanak, and T. D. Veal, APL Mater. **7**, 022528 (2019).
[42]P. Weiser, M. Stavola, W. B. Fowler, Y. Qin, and S. Pearton, Appl. Phys. Lett. **112**, 232104 (2018).
[43]J. B. Varley, H. Peelaers, A. Janotti, and C. G. V. de Walle, J. Phys.: Condens. Matter **23**, 334212 (2011).
[44]P. D. C. King, I. McKenzie, and T. D. Veal, Appl. Phys. Lett. **96**, 062110 (2010).
[45]J. B. Varley, J. R. Weber, A. Janotti, and C. G. V. de Walle, Appl. Phys. Lett. **97**, 142106 (2010).
[46]J. R. Ritter, J. Huso, P. T. Dickens, J. B. Varley, K. G. Lynn, and M. D. McCluskey, Appl. Phys. Lett. **113**, 052101 (2018).
[47]C. Pansegrau, J. Jesenovec, J. S. McCloy, and M. D. McCluskey, Appl. Phys. Lett. **119**, 102104 (2021).
[48]M. Higashiwaki and S. Fujita, *Gallium Oxide* (Springer International Publishing, 2020).
[49]M. E. Ingebrigtsen, A. Y. Kuznetsov, B. G. Svensson, G. Alfieri, A. Mihaila, and L. Vines, J. Appl. Phys. **125**, 185706 (2019).
[50]A. Y. Polyakov, I.-H. Lee, A. Miakonkikh, A. V. Chernykh, N. B. Smirnov, I. V. Shchemerov, A. I. Kochkova, A. A. Vasilev, and S. J. Pearton, J. Appl. Phys. **127**, 175702 (2020).

[51]A. Y. Polyakov, N. B. Smirnov, I. V. Shchemerov, A. A. Vasilev, E. B. Yakimov, A. V. Chernykh, A. I. Kochkova, P. B. Lagov, Y. S. Pavlov, O. F. Kukharchuk, A. A. Suvorov, N. S. Garanin, I.-H. Lee, M. Xian, F. Ren, and S. J. Pearton, J. Phys. D: Appl. Phys. **53**, 274001 (2020).
[52]H. Aida, K. Nishiguchi, H. Takeda, N. Aota, K. Sunakawa, and Y. Yaguchi, Jpn. J. Appl. Phys. **47**, 8506 (2008).
[53]A. Kuramata, K. Koshi, S. Watanabe, Y. Yamaoka, T. Masui, and S. Yamakoshi, Jpn. J. Appl. Phys. **55**, 1202A2 (2016).
[54]See https://www.tamuracorp.com/products/gao/index.html for "Tamura Corporation: β-Ga_2O_3 Crystals Grown by Edge-Defined Film-Fed Growth" (2020); accessed 12 May 2020.
[55]M. Stavola and W. B. Fowler, J. Appl. Phys. **123**, 161561 (2018).
[56]M. E. Ingebrigtsen, L. Vines, G. Alfieri, A. Mihaila, U. Badstübner, B. G. Svensson, and A. Kuznetsov, Mater. Sci. Forum **897**, 755 (2017).
[57]M. Passlack, N. E. J. Hunt, E. F. Schubert, G. J. Zydzik, M. Hong, J. P. Mannaerts, R. L. Opila, and R. J. Fischer, Appl. Phys. Lett. **64**, 2715 (1994).
[58]B. G. Svensson, K.-H. Rydén, and B. M. S. Lewerentz, J. Appl. Phys. **66**, 1699 (1989).
[59]A. A. Istratov, J. Appl. Phys. **82**, 2965 (1997).
[60]D. V. Lang, J. Appl. Phys. **45**, 3023 (1974).
[61]P. E. Blöchl, Phys. Rev. B **50**, 17953 (1994).
[62]G. Kresse and D. Joubert, Phys. Rev. B **59**, 1758 (1999).
[63]A. V. Krukau, O. A. Vydrov, A. F. Izmaylov, and G. E. Scuseria, J. Chem. Phys. **125**, 224106 (2006).
[64]G. Kresse and J. Furthmüller, Phys. Rev. B **54**, 11169 (1996).
[65]J. Åhman, G. Svensson, and J. Albertsson, Acta Crystallogr. C Cryst. Struct. Commun. **52**, 1336 (1996).
[66]C. Freysoldt, B. Grabowski, T. Hickel, J. Neugebauer, G. Kresse, A. Janotti, and C. G. V. de Walle, Rev. Mod. Phys. **86**, 253 (2014).
[67]C. Freysoldt, J. Neugebauer, and C. G. V. de Walle, Phys. Rev. Lett. **102**, 016402 (2009).
[68]Y. Kumagai and F. Oba, Phys. Rev. B **89**, 195205 (2014).
[69]T. Gake, Y. Kumagai, C. Freysoldt, and F. Oba, Phys. Rev. B **101**, 020102 (2020).
[70]A. M. Stoneham, *Theory of Defects in Solids* (Oxford University, 1975).
[71]D. Wickramaratne, C. E. Dreyer, B. Monserrat, J.-X. Shen, J. L. Lyons, A. Alkauskas, and C. G. V. de Walle, Appl. Phys. Lett. **113**, 192106 (2018).
[72]A. Alkauskas, M. D. McCluskey, and C. G. V. de Walle, J. Appl. Phys. **119**, 181101 (2016).
[73]G. Henkelman, B. P. Uberuaga, and H. Jansson, J. Chem. Phys. **113**, 9901 (2000).
[74]J. Sun, A. Ruzsinszky, and J. Perdew, Phys. Rev. Lett. **115**, 036402 (2015).
[75]A. Kuramata, K. Koshi, S. Watanabe, and Y. Yamaoka, "Floating zone method, edge-defined film-fed growth method, and wafer manufacturing," in *Gallium Oxide: Materials Properties, Crystal Growth, and Devices*, edited by M. Higashiwaki and S. Fujita (Springer International Publishing, Cham, 2020), pp. 57–75.
[76]J. B. Varley, "First-principles calculations 2," in *Gallium Oxide: Materials Properties, Crystal Growth, and Devices*, edited by M. Higashiwaki and S. Fujita (Springer International Publishing, Cham, 2020), pp. 329–348.
[77]Y. K. Frodason, C. Zimmermann, E. F. Verhoeven, P. M. Weiser, L. Vines, and J. B. Varley, Phys. Rev. Mater. **5**, 025402 (2021).
[78]P. W. Anderson, Phys. Rev. Lett. **34**, 953 (1975).
[79]C. G. Hemmingsson, N. T. Son, A. Ellison, J. Zhang, and E. Janzén, Phys. Rev. B **58**, R10119 (1998).
[80]V. M. Reinertsen, P. M. Weiser, Y. K. Frodason, M. E. Bathen, L. Vines, and K. M. Johansen, Appl. Phys. Lett. **117**, 232106 (2020).
[81]W. B. Fowler, M. Stavola, Y. Qin, and P. Weiser, Appl. Phys. Lett. **117**, 142101 (2020).
[82]J. L. Lyons, Semicond. Sci. Technol. **33**, 05LT02 (2018).
[83]Y. K. Frodason, K. M. Johansen, L. Vines, and J. B. Varley, J. Appl. Phys. **127**, 075701 (2020).
[84]M. W. Swift, H. Peelaers, S. Mu, J. J. L. Morton, and C. G. V. de Walle, npj Computat. Mater. **6**, 181 (2020).